



Published in final edited form as:

*J Inorg Biochem.* 2020 May ; 206: 110997. doi:10.1016/j.jinorgbio.2020.110997.

## Hydrolyzed Ce(IV) Salts Limit Sucrose-Dependent Biofilm Formation by *Streptococcus mutans*

Lopa Bhatt<sup>1</sup>, Lin Chen, Jinglong Guo<sup>2,1</sup>, Robert F. Klie<sup>1</sup>, Junhe Shi, Russell P. Pesavento<sup>2,3,\*</sup>

<sup>1</sup>Department of Physics, University of Illinois at Chicago, 801 S. Paulina Street, Chicago, IL, 60612, USA

<sup>2</sup>Center for Wound Healing and Tissue Regeneration, College of Dentistry, University of Illinois at Chicago, 801 S. Paulina Street, Chicago, IL, 60612, USA

<sup>3</sup>Department of Oral Biology, College of Dentistry, The Center for Biomolecular Sciences and Department of Medicinal Chemistry and Pharmacognosy, University of Illinois at Chicago, 801 S. Paulina Street, Chicago, IL, 60612, USA

### Abstract

Several studies have focused on the antimicrobial effects of cerium oxide nanoparticles (CeO<sub>2</sub>-NP) but few have focused on their effects on bacteria under initial biofilm formation conditions. *Streptococcus mutans* is a prolific biofilm former contributing to dental caries in the presence of fermentable carbohydrates and is a recognized target for therapeutic intervention. CeO<sub>2</sub>-NP derived solely from Ce(IV) salt hydrolysis were found to reduce adherent bacteria by approximately 40% while commercial dispersions of “bare” CeO<sub>2</sub>-NP (*e.g.*, 3 nm, 10–20 nm, 30 nm diameter) and Ce(NO<sub>3</sub>)<sub>3</sub>•6H<sub>2</sub>O were either inactive or observed to slightly increase biofilm formation under similar *in vitro* conditions. Planktonic growth and dispersal assays support a non-bactericidal mode of biofilm inhibition active in the initial phases of *S. mutans* biofilm production. Human cell proliferation assays suggest only minor effects of hydrolyzed Ce(IV) salts on cellular metabolism at concentrations up to 1 mM Ce, with less observed toxicity compared to equimolar concentrations of AgNO<sub>3</sub>. The results presented herein have implications in clinical dentistry.

### Keywords

Ce(IV); biofilm; inhibition; dental; *Streptococcus mutans*

## 1. INTRODUCTION

The composition of clinically relevant biofilms varies significantly depending on the tissue, host and local environment. The oral cavity is home to a diverse array of microorganisms

\*To whom correspondence should be addressed: rpesaven@uic.edu.

### Credit Author Statement:

RPP - Conceptualization, original manuscript draft, carried out all bacterial based biological assays, synthetic preparations and DLS analysis. LC and JS - carried out the human cell proliferation studies, data analysis and manuscript editing. RFK, LB and JG - carried out the STEM/EELS studies, data analysis and manuscript editing. All authors read and approved manuscript prior to submission.

(i.e., oral microbiome) with varying capacities to form biofilms [1]. *Streptococcal mutans* is among the robust tooth-adhering biofilm formers in the presence of fermentable carbohydrates (e.g., sucrose). This strong capacity for biofilm production by *S. mutans* is associated with both tooth decay and bacterial endocarditis [2]. As such, *S. mutans* has long been the target of antimicrobial therapy to limit tooth decay and associated comorbidities [3]. Inorganic tooth-applied agents (e.g., AgNO<sub>3</sub>, silver diamine fluoride) are effective at arresting tooth decay, yet they are non-selective bactericidal agents whose repeated administration has raised concerns of emerging bacterial resistance [4, 5] and deleterious effects on the oral microbiota. Although agents with selective toxicity for highly cariogenic species are welcomed, none are currently available for clinical use. As such, tooth-applied biofilm inhibitors with non-lethal mechanisms of action have defined the search in preventive dentistry with the aim of limiting the effects on the entirety of the oral microbiome.

The use of nanoparticles in preventive and restorative dentistry has received considerable interest in recent years [6, 7]. Cerium oxide nanoparticles (CeO<sub>2</sub>-NP) are an attractive option for oral application due to their diverse range of sizes and morphologies attributed to variations in synthetic methodology [8]. This morphological diversity may be harnessed into differential medicinal activity [8]. Although the antimicrobial activity of CeO<sub>2</sub>-NP has been the subject of several studies and a recent review [9], their effects on established biofilm communities have only been reported recently [10–13]. Fewer studies have focused on the interaction of sublethal concentrations of CeO<sub>2</sub>-NP with bacteria under the initial biofilm forming conditions. Masadeh et al. [14] recently concluded that CeO<sub>2</sub>-NP (25–50 nm) were inactive as biofilm inhibitors and they also reduced the activity of known antimicrobial agents against a panel of selected bacteria. Xu et al. reported that CeO<sub>2</sub>-NP (50 nm) accelerated *in vitro* biofilm formation in *P. aeruginosa* [15]. It was postulated that bacterial exposure to “bare” CeO<sub>2</sub>-NP of this size increased cell surface hydrophobicity, aggregation and the production of reactive oxygen species (ROS) potentiating quorum sensing pathways and enhancing biofilm production [15, 16]. The goal of the present study was to expand upon the literature regarding CeO<sub>2</sub>-NP as biofilm inhibitors. CeO<sub>2</sub>-NP prepared from Ce(IV) salt hydrolysis [17–20] were screened against “bare” CeO<sub>2</sub>-NP of variable size and Ce(NO<sub>3</sub>)<sub>3</sub>•6H<sub>2</sub>O for their ability to perturb initial *in vitro* biofilm formation of the clinically relevant pathogen, *S. mutans*. The aggregation and dispersion properties of similarly sized CeO<sub>2</sub>-NP obtained from different synthetic methodology were also investigated offering insight into the variable biological activity observed.

## 2. RESULTS AND DISCUSSION

### 2.10 *In vitro* Adherent Bacteria Assays

The initial screen for *S. mutans* biofilm inhibition was carried out utilizing 125 μM Ce-containing agents of varying properties on a polystyrene (PS) plate (See Figure 1). All Ce-containing solutions were prepared as 5 mM (Ce ion) stock solutions (aged <30 min) at room temperature (rt) for consistency and diluted to 125 μM in brain heart infusion (BHI) media containing cells (and 1% sucrose) grown to log phase. It should be noted that no statistical difference in inhibitory activity was found when hydrolyzed Ce(IV) salts were

allowed to age 20 h (at rt) prior to the static biofilm inhibition assays. Commercial dispersions of “bare” CeO<sub>2</sub>-NP: 3 nm solution diameter (Strem, 20% dispersion, pH 3.5 ± 0.75), 10–20 nm solution diameter (Alfa Aesar, 20% dispersion, pH 1.5), 30 nm (Alfa Aesar, 15% dispersion) and Ce(NO<sub>3</sub>)<sub>3</sub>•6H<sub>2</sub>O were either inactive or slightly increased biofilm growth of *S. mutans* at 20 h under the above conditions. In contrast, both hydrolyzed CAN (ceric ammonium nitrate) and CAS (ceric ammonium sulfate) displayed a significant reduction in adherent cells (approximately 40%) of *S. mutans* (See Figure 1). Further, dilution of a 1N solution of H<sub>2</sub>[Ce(NO<sub>3</sub>)<sub>6</sub>] similar to reported methods known to produce CeO<sub>2</sub>-NP [17] was found to limit biofilm growth of *S. mutans* comparable to CAN and CAS (data not shown). No inhibition was observed with either 1 mM NH<sub>4</sub>NO<sub>3</sub> (AN) or (NH<sub>4</sub>)<sub>2</sub>SO<sub>4</sub> (AS), the byproducts of ceric ammonium salt hydrolysis. The addition of 4 equivalents of AS to stock solutions containing any of the commercially prepared CeO<sub>2</sub>-NP (3 nm, 10–20 nm, 30 nm) did not result in increased biofilm inhibition. Further, balancing both the nitrate content and acidity of a CeO<sub>2</sub>-NP (3nm, Strem) dispersion (with 4M HNO<sub>3</sub>) to an equivalent amount present in H<sub>2</sub>[Ce(NO<sub>3</sub>)<sub>6</sub>] did not result in a statistically significant increase in biofilm inhibition at 125 μM (Ce).

### 2.11 Fluorescence Microscopy of Adherent Biofilm

Light microscopy with fluorescent labeling further supported disruption of *S. mutans* biofilm formation by hydrolyzed Ce(IV) salts. SYPRO™ Ruby Biofilm Matrix Stain (Invitrogen) was used to stain the adherent biofilm post-wash according manufacturers protocol. Reduction in adherent biofilm was observed in the treated wells (250 μM CAS) as compared to the positive control in Figure 2.

### 2.12 Planktonic Cellular Growth Curve Analysis

The planktonic growth of *S. mutans* in BHI (37°C, 5% CO<sub>2</sub>) was measured in 30 min intervals in the presence of 500 μM CAN and CAS over 10 h (See Figure 3). Figure 3 shows that 500 μM CAS had a minimal effect on the planktonic growth of *S. mutans*, while CAN had a lagging effect on the planktonic growth rate that becomes comparable with the positive control over several h. The concentration of CAN and CAS in this assay was 500 μM, approximately *four-fold* the concentration utilized in the initial screening assay in the same growth media (BHI). Thus, the significant reduction in adherent bacteria observed in the initial screening assay (Figure 1) is attributed to non-bactericidal mechanism(s).

### 2.13 Dose Dependence Adherent Bacteria Reduction (IC<sub>50</sub> determination)

A dose response curve was developed quantifying the effects of varying concentrations (0 – 1 mM) of CAN on the adherent cells of *S. mutans* grown under similar conditions utilized in the initial screening assay (37 °C, 5% CO<sub>2</sub>, 1% sucrose) (See Supplemental Data, Figure S1). The IC<sub>50</sub> value for reduction in adherent bacteria is 137 μM (± 24 μM) CAN. This demonstrates that the reduction in adherent cells under the initial phase of biofilm growth is directly proportional to the concentration of CAN present.

### 2.14 Bacterial Cell Viability Assay

The above results prompted further studies on the effects of higher concentrations of hydrolyzed Ce(IV) salts (1 mM) on the planktonic growth of two different and related bacteria that reside in the human oral cavity. *S. mutans* and *S. sobrinus* 6175 were exposed to 1 mM CAN, CAS or AgNO<sub>3</sub> in BHI growth media and allowed to grow 20 h (See Table I) under similar conditions (no sucrose added) of the initial screening assay. Visible turbidity (++) was noticeable in all wells containing either 1 mM CAN or CAS after 20 h. In contrast, wells containing 1 mM AgNO<sub>3</sub> showed no visible signs (--) of growth. The results demonstrate that both CAN and CAS do not inhibit *S. mutans* or *S. sobrinus* growth at 1 mM (Ce) in BHI, nearly *eight times* the concentration utilized in the initial screening assay.

### 2.15 Biofilm Dispersal Assay

Biofilm dispersal assays [21] were carried out to investigate if hydrolyzed Ce(IV) salts can disrupt the immature biofilm matrix produced by *S. mutans*. The use of 500 μM CAS as a dispersal agent resulted in a non-statistically significant reduction of adherent bacteria compared to the positive control. The dispersal assay was carried out with a CAS concentration *four times* that utilized in the initial screening assay described above. Non-targeted chemical disruption of the biomolecular components of the biofilm matrix by CAS as a mechanism of adherent cell reduction is unlikely, as a significant dispersal rate would have been achieved in this experiment. Instead, it is likely the hydrolyzed Ce(IV) salts target specific cellular events or biomolecules critical to the initial phases of biofilm formation.

### 2.16 Sucrose Metabolism Assay (Acid Production)

CeO<sub>2</sub>-NP exhibit enzymatic activity based upon their surface oxidation state(s) and size when present in the media of interest [22]. Sucrose is a both a building block for the synthesis of extracellular polysaccharides and an energy source for *S. mutans*. A sucrose metabolism assay was carried out to test if the hydrolyzed Ce(IV) salts irreversibly modify sucrose in complex growth media so as to prevent its metabolism. Phenol Red Broth Base media was chosen both to limit media acidification due to the metabolism of other manufacturer added carbohydrates [23] as well as to mimic the properties of the BHI. At both 5 and 20 h incubation, a similar media acidification was observed (See Supplemental Data, Table S1) among the positive control and the Ce(IV) treated media. It is unlikely that the hydrolyzed Ce(IV) salts are irreversibly modifying sucrose to limit its metabolism in growth media.

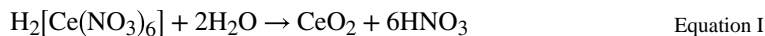
### 2.17 Human Cell Proliferation Assays

A human cell proliferation assay (24 h) was carried out testing the effects of hydrolyzed Ce(IV) salts and AgNO<sub>3</sub> (0–1 mM) on the metabolic activity of oral derived human cells, TIGK and HGF. AgNO<sub>3</sub> was used as the standard of clinical comparison, as it is utilized as a tooth-applied caries arresting agent. Similar metal ion concentrations of both CAN and CAS had less overall effect on the metabolic activity of TIGKs and HGFs as compared to AgNO<sub>3</sub>. As shown in Figure 4, treatment of both human cell populations with equimolar doses of AgNO<sub>3</sub> was consistent with statistically more cytotoxicity as compared to equivalent doses of hydrolyzed Ce(IV) salts CAN and CAS. It should be noted that intraoral application of

Ag-containing agents are often applied at significantly higher concentrations than shown below.

### 2.18 Dynamic Light Scattering (DLS) Studies

The hydrolysis of CAN or  $[\text{Ce}(\text{NO}_3)_6]^{2-}$  yields an acidic solution with six equivalents of  $\text{NO}_3^-$  per one equivalent of Ce (*See* Equation I). Raising the pH of  $\text{CeO}_2$ -NP obtained from Ce(IV) hydrolysis to remove adsorbed  $\text{NO}_3^-$  leads to aggregation and precipitation [17, 19]. A 5 mM solution of  $[\text{Ce}(\text{NO}_3)_6]^{2-}$  (or CAN) produces 30 mM  $\text{NO}_3^-$  upon hydrolysis, which must be accounted for in the DLS analysis. The commercially available  $\text{CeO}_2$ -NP screened for biological activity have zero (or limited)  $\text{NO}_3^-$  present in the dispersion. Thus, the commercially supplied  $\text{CeO}_2$ -NP dispersions were diluted to a concentration of 5 mM Ce and 30 mM  $\text{KNO}_3$  to provide a consistent  $\text{NO}_3^-$  containing media for all species tested (*See* Supplemental Data, Figures S2 A–E) with little change to the existing pH found upon simple dilution.



Both CAN and  $[\text{Ce}(\text{NO}_3)_6]^{2-}$  (with 30 mM  $\text{NO}_3^-$ ) had average peak hydrodynamic diameters of approximately 9–10 nm (*See* Supplemental Data, Figures S2 A–B).  $\text{CeO}_2$ -NP's prepared from Ce(IV) hydrolysis (*e.g.*  $[\text{Ce}(\text{NO}_3)_6]^{2-}$ ) had a narrowed intensity distribution compared to commercially available  $\text{CeO}_2$ -NP of similar size (3 nm, Strem) in 30 mM  $\text{KNO}_3$  (*See* Figure 5). Figure 6 illustrates the effect of a more strongly coordinating media (+ 40 mM KCl) on the hydrodynamic diameter and distribution of  $[\text{Ce}(\text{NO}_3)_6]^{2-}$  vs  $\text{CeO}_2$ -NP (3 nm, Strem) in acidic media (*See* Figure 6). At pH 7.4 (50 mM  $\text{KH}_2\text{HPO}_4$ )  $\text{CeO}_2$ -NP prepared from the hydrolysis of  $[\text{Ce}(\text{NO}_3)_6]^{2-}$  aggregate to form a monodispersed distribution (Figure 7) with limited stability over several h. Under the same pH conditions,  $\text{CeO}_2$ -NP (3nm, Strem) fails to form an interpretable dispersion. It should be noted the average pH of the BHI (growth media) utilized in the cell based experiments is approximately 7.4.

### 2.19 Scanning Transmission Electron Microscopy (STEM) and Electron Energy-Loss Spectroscopy (EELS)

$\text{CeO}_2$ -NP prepared by  $[\text{Ce}(\text{NO}_3)_6]^{2-}$  hydrolysis and “bare”  $\text{CeO}_2$ -NP (3 nm, Strem) were encapsulated in graphene liquid cells [24] for STEM high-angle annular dark-field (HAADF) imaging and EELS analysis. The low-magnification HAADF images of hydrolyzed  $[\text{Ce}(\text{NO}_3)_6]^{2-}$  and  $\text{CeO}_2$ -NP (3nm, Strem) are shown in Figures 8a–b, respectively. We find that compared with  $\text{CeO}_2$ -NP (3nm, Strem),  $\text{CeO}_2$ -NP prepared by  $[\text{Ce}(\text{NO}_3)_6]^{2-}$  hydrolysis tend to aggregate more, even after the samples are diluted significantly during the sample preparation process. Atomic-resolution HAADF images of the aggregated  $\text{CeO}_2$ -NP are shown as insert in Figure 8a–b. The lattice fringes of the  $\text{CeO}_2$  nanoparticles can be clearly seen, indicating that the  $\text{CeO}_2$ -NP are fully crystalline. We do not observe any amorphous surface layer in either sample tested. Detailed analysis of many HAADF images reveal that the particle size in both samples is 3.5 nm on average, with a very narrow particle size distribution. To confirm the oxidation state of aqueous dispersed

CeO<sub>2</sub>-NP, we performed EELS on CeO<sub>2</sub>-NP encapsulated within the graphene liquid cells. Specifically, we have used the Ce *M*-edges to determine the Ce valence state. The Ce *M*-edge splits into two prominent peaks, the M<sub>5</sub> and the M<sub>4</sub> edges due to spin-orbit coupling of the initial states. Previous reports of Ce valence state analysis using EELS have found that the Ce M<sub>5</sub>/M<sub>4</sub> ratio closely tracks with the Ce oxidation state, where the M<sub>4</sub> peak shows a higher intensity than the M<sub>5</sub> peak for Ce(IV), while the M<sub>4</sub> peak is lower in intensity than the M<sub>5</sub> peak in Ce(III) [24, 25]. The Ce *M*-edge spectra for both samples are shown in Figure 1c) and d) showing a higher intensity of the M<sub>4</sub> peak, corresponding to a Ce(IV) (*i.e.* fully stoichiometric CeO<sub>2</sub>). We need to point out that for CeO<sub>2</sub>-NP not dispersed in solution, but rather exposed to the vacuum of the transmission electron microscopy (TEM) column, we find that the valence state is reduced to Ce(III), as expected for particles with an average size of 3.5 nm [25]

## 2.20 CeO<sub>2</sub>-NP Surface Properties and Biological Activity

The most suitable comparison between CeO<sub>2</sub>-NP utilized in this study is between hydrolyzed [Ce(NO<sub>3</sub>)<sub>6</sub>]<sup>2-</sup> and CeO<sub>2</sub>-NP (3nm, Strem) due to the equivalent size (avg 3.5 nm), predominately Ce(IV) oxidation state and absence of ammonium ions. Hydrolyzed [Ce(NO<sub>3</sub>)<sub>6</sub>]<sup>2-</sup> are *more* stable at both higher ionic strength and as an aggregate at pH (7.4) compared to CeO<sub>2</sub>-NP (3 nm, Strem). This underscores the idea that differential surface reactivity and aggregation properties exists between the two species of CeO<sub>2</sub>-NP. This is likely brought about by the different synthetic methodology, specifically, the use of a high valent Lewis acid salt as a starting material with no further manipulation yielding strongly acidic media, excess absorbable anions and a high surface area. [17]. It is likely the enhanced *in vitro* biofilm inhibiting capacity observed with hydrolyzed Ce(IV) salts reflects their differential surface reactivity and/or stability towards the biomolecular components of the growth media. This includes the potential for variable release and/or reduction of Ce(IV) ions on the CeO<sub>2</sub>-NP surface [10]. It has been previously observed that the protein (or biomolecular) corona on the surface of metal oxide NPs has a significant influence on the resultant biological activity [26, 27]. In the present study, it was found that rigorous mixing of hydrolyzed Ce(IV) salts in the growth media prior to initiation of adherent bacteria assays reduced their inhibitory activity - supporting a significant role of both surface reactivity and the protein corona on the observed biological activity. This study sets forth that the mechanism of biofilm inhibition by hydrolyzed Ce(IV) salts is non-bactericidal at the concentrations tested and likely targets the initial phases critical to biofilm formation. Further, the mechanism of inhibition does not support irreversible reactivity of CeO<sub>2</sub>-NP with sucrose or non-targeted chemical disruption of the macromolecular components of the extracellular matrix as the predominate mode of biofilm inhibition. Current studies are underway to investigate not only the chemical reactivity with biological media components but also a relevant biological mechanism of activity.

## 3. CONCLUSIONS

CeO<sub>2</sub>-NP of variable size and synthetic methodology were screened for the *in vitro* reduction of adherent *S. mutans* biofilm formation in complex growth media. While commercially available “bare” CeO<sub>2</sub>-NP were ineffective at reducing adherent cells at the

concentrations tested, hydrolyzed Ce(IV) salts prepared in strongly acidic media were active as *in vitro* biofilm inhibitors ( $IC_{50} = 137 \mu\text{M}$ ). The inhibition likely takes place in the initial phases of biofilm formation and under a non-bactericidal mechanism. Differences in biofilm inhibition between hydrolyzed Ce(IV) salts and commercially prepared CeO<sub>2</sub>-NP of similar size (3.5 nm), distribution and oxidation state [Ce(IV)] are not attributed *directly* to the storage solution acidity, exogenous ions (e.g., NH<sub>4</sub>, NO<sub>3</sub><sup>-</sup>, etc.) or cytotoxicity. Further mechanistic studies are underway focusing on both the chemical and biological aspects of biofilm inhibition of *S. mutans* and related species.

## 4. MATERIALS AND METHODS

All chemical reagents were purchased commercially and utilized without further purification. Ultrapure Milli-Q® water was used to prepare all samples for Dynamic Light Scattering (DLS), TEM data collection and UV-Vis Spectroscopy. Ceric ammonium nitrate hexahydrate (99.9%) (CAN) was purchased from Sigma-Aldrich, ceric ammonium sulfate dihydrate (98%) (CAS) was purchased from Acros and Ce(NO<sub>3</sub>)<sub>3</sub>•6H<sub>2</sub>O (99.5%) was purchased from Alfa Aesar. Ceric nitrate (1.0 N aqueous solution) was purchased from GFS Chemicals (Columbus, Ohio). Commercially available “bare” cerium oxide nanoparticles (CeO<sub>2</sub>-NP) were purchased and stored as the following colloidal dispersions: (1) Strem Chemicals (Newbury MA), 3nm diameter (DLS) CeO<sub>2</sub>-NP, stored as an acidic dispersion at pH  $3.5 \pm 0.75$ , (2) Alfa Aesar (Ward Hill, MA) 10–20 nm diameter (DLS) CeO<sub>2</sub>-NP (20%), stored as an acidic dispersion at pH 1.5 with 0.2 mol NO<sub>3</sub> per mole, and (3) Alfa Aesar, 30 nm diameter (APS) CeO<sub>2</sub>-NP (15%). AgNO<sub>3</sub> and NH<sub>4</sub>NO<sub>3</sub> were purchased from Ward’s Science and KNO<sub>3</sub>, KCl and (NH<sub>4</sub>)<sub>2</sub>SO<sub>4</sub> were purchased from Fisher Scientific. Disposable BrandTech PMMA cuvettes (Cole-Parmer, Vernon Hills, IL) were used for Dynamic Light Scattering (DLS) measurements. Bacterial cultures were prepared from frozen glycerol stocks of each species of *Streptococcus mutans* (UA159) *Streptococcus sobrinus* (6175) in either sterilized Brain Heart Infusion (BHI) growth media (Criterion) or Phenol Red Broth Base (Sigma-Aldrich). All pH measurements were carried out on a Mettler Toledo FE20 benchtop pH meter following acidic and neutral pH calibration.

### 4.10 Hydrolysis/Dilution of Ce(IV) Salts

CeO<sub>2</sub>-NP from Ceric Ammonium Nitrate. Following a similar preparation reported by Pettinger *et. al.* [19], ceric ammonium nitrate hexahydrate (Aldrich, 13.7 mgs) (CAN) was dissolved in 5.0 mL of deionized water at room temperature (rt) with gentle mixing for 20 s to afford a 5 mM (Ce) stock solution. The faint-orange colored solution faded within min to yield a clear dispersion. The UV-Vis absorption spectrum of CAN (NanoDrop™ 2000/2000c, Thermo Fisher) in H<sub>2</sub>O (150 μM Ce) was in agreement with the literature, with a well-defined shoulder peak at 290 nm that intensifies significantly upon standing in solution over several h and an intense peak at approximately 230 nm is attributed to the absorption of NO<sub>3</sub><sup>-</sup> [19]. (See Supplemental Data, Figure S3)

CeO<sub>2</sub>-NP from Ceric Ammonium Sulfate. A 5 mM (Ce) stock solution of ceric ammonium sulfate dihydrate (CAS) was prepared by dissolving CAS (15.8 mgs) in 5.0 mLs of deionized (DI) water at rt with gentle mixing for 20 s to produce an acidic dispersion of

CeO<sub>2</sub>-NP. The yellow tinted color faded within s to produce a clear dispersion. The UV-Vis absorption spectrum of CAS in H<sub>2</sub>O (150 μM Ce) lacked a well-defined peak at 290 nm (and 230 nm) previously observed with CAN. Instead, a broadened peak with an absorption maximum at 275 nm was observed. (*See Supplemental Data, Figure S3*).

CeO<sub>2</sub>-NP from Ceric Nitrate. A 5 mM (Ce) stock solution of ceric nitrate (H<sub>2</sub>[Ce(NO<sub>3</sub>)<sub>6</sub>]) was prepared by diluting a 1.0 N solution of H<sub>2</sub>[Ce(NO<sub>3</sub>)<sub>6</sub>] (25μL) to 5.0 mL with 4.975 mL of DI water at rt with gentle mixing to produce an acidic dispersion of CeO<sub>2</sub>-NP [17]. The deep yellow color faded over several min to produce a clear, acidic dispersion of CeO<sub>2</sub>-NP.

#### 4.11 Dynamic light scattering (DLS)

All size vs intensity data was collected at the UIC Nanotechnology Core Facility (NCF) utilizing a Malvern Zetasizer ZSP. The hydrodynamic diameter of each Ce-containing sample was collected as a function of intensity weighted distribution in a 30 mM NO<sub>3</sub><sup>-</sup> buffer prepared in Milli-Q® water (18.2 MΩ). CAN and H<sub>2</sub>[Ce(NO<sub>3</sub>)<sub>6</sub>] were dissolved in Milli-Q® water to yield solutions containing 5 mM Ce and 30 mM NO<sub>3</sub><sup>-</sup>. Commercially “bare” dispersions of CeO<sub>2</sub>-NP were diluted with 30 mM KNO<sub>3</sub> solutions. This step was carried out to provide a consistent level of NO<sub>3</sub><sup>-</sup> in each Ce-containing sample for DLS analysis. Both CAN and H<sub>2</sub>[Ce(NO<sub>3</sub>)<sub>6</sub>] yield six moles of NO<sub>3</sub><sup>-</sup> present per each mole of Ce(IV) present, while commercially available, “bare” CeO<sub>2</sub>-NP (Strem, Alfa Aesar) have zero (or small amounts) NO<sub>3</sub><sup>-</sup> present. Following standing at rt for 30–40 min, each Ce-containing sample was then vortexed for 2 min before being transferred into a polymethylmethacrylate (PMMA) disposable cuvette for an initial analysis (*Supplemental Data, Figures S2A–E*). Additionally, a solution of KCl was added to stock solutions of H<sub>2</sub>[Ce(NO<sub>3</sub>)<sub>6</sub>] and CeO<sub>2</sub>-NP (3 nm, Strem) in 30 mM NO<sub>3</sub><sup>-</sup> to afford a higher ionic strength buffer with stronger coordinating ligands (40 mM KCl) (*Figure 6*). All size measurements were carried out with a minimum of 12 replicates and reported as an average intensity weighted distribution utilizing a 633 nm laser and a backscattering angle of 173°.

#### 4.12 High Resolution Transmission Electron Microscopy (HR-TEM), STEM and EELS

HR-TEM images were recorded by a JEOL JEM-3010 microscope (operating at 300 kV) equipped with a Gatan Orius CCD camera for imaging and a Thermal-Noran XEDS detector. Solutions of CAN and CAS (5 mM) were dissolved in Ultrapure Milli-Q water, vortexed gently and allowed to stand approximately 20 h at rt prior to recording images. Dispersions were then further diluted 5-fold and to a concentration of approximately 1 mM Ce and pipetted (3–5 μL) onto a 400 Cu square mesh holey carbon TEM grid (21, 22). Excess water from the grid was wicked away and then dried in a vacuum desiccator for a minimum of 30 min prior to HR-TEM image collection (*See Supplemental Data, Figures S4–S5*). The atomic resolution Z-contrast images and EELS maps were collected using the JEOL ARM200CF aberration corrected STEM with a cold-field emission gun operated at an acceleration voltage of 80 kV. The HAADF images were acquired using an annular dark-field detector with a collection angle ranging from 90 to 175 mrad. The probe convergence semi-angle was set to 29 mrad, which yields a probe size of 1 Å at 80 kV and a probe current of 62 pA. EELS characterization was conducted using the post-column Gatan Continuum GIF spectrometers. Samples were encapsulated in graphene liquid cells with



aqueous media as previously reported [28–31].  $\text{H}_2[\text{Ce}(\text{NO}_3)_6]$  and  $\text{CeO}_2\text{-NP}$  (3 nm, Strem) samples were diluted to 5 mM (Ce) in Ultrapure Milli-Q water and stored at cold temperature prior to encapsulation.

#### 4.13 *In vitro* Adherent Bacteria Assay

An overnight culture of *S. mutans* UA159 was diluted and grown to mid exponential growth phase ( $\text{OD}_{600} = 0.5\text{--}0.6$ ) in Brain Heart Infusion (BHI) growth media. The cells were diluted 40-fold into a BHI/1% sucrose solution and transferred to a 96-well, tissue cultured, polystyrene (PS) microtiter plate. The wells of the microtiter plate were inoculated with freshly diluted BHI containing *S. mutans* and 1% sucrose and each appropriate stock solution to afford either 125  $\mu\text{M}$  Ce containing agents or 1 mM  $\text{NH}_4\text{NO}_3/(\text{NH}_4)_2\text{SO}_4$  to a total volume of 200  $\mu\text{L}$  in each well. All stock solutions were prepared (hydrolyzed or diluted) within 30 min of addition to each microtiter plate. The wells were mixed gently with a microchannel pipette following addition of each agent. Both experimental and control wells were set up with six replicates. The microtiter plate was then placed in an incubator under the following conditions: 37°C, 5%  $\text{CO}_2$  for 20 h in the absence of light. Following the 20 h incubation time, the plates were gently submerged in a water bath 3–4 times to remove excess non-adherent cells and cellular debris. Each well was then stained with 200  $\mu\text{L}$  of 0.1% crystal violet (CV) stain for approximately 30 min at 37°C. The microtiter plate was then gently re-submerged (washed) in a deionized water bath, to remove excess dye and dry for a minimum of 24 h. The dyed contents of each well were re-dissolved in 33% acetic acid with repeated mixing and diluted with DI water. The absorbance of each well at 570 nm ( $\text{ABS}^{570}$ ) was then recorded with a Victor3v plate reader, and the average absorbance of the six replicates were recorded. The ratio of the adherent bacteria present in the test wells vs. the positive control was determined by Equation II and plotted in Figure 1 as the mean  $\pm$  SD. Note negative control absorbances at 570 nm were subtracted from each positive control and test well value.

$$\text{Adherent Bacteria Ratio} = \left[ \frac{(\text{ABS}^{570}_{\text{test well}})}{(\text{ABS}^{570}_{+\text{control}})} \right] \quad \text{Equation II}$$

#### 4.14 Fluorescence Microscopy of Adherent Biofilm

Lab-Tek® Chamber slide (8-well Permacol® Slide) was inoculated with *S. mutans* (BHI, 1% sucrose) in a manner similar as described above. The wells were run in duplicate, incorporating positive and negative controls, as well as 125  $\mu\text{M}$  and 250  $\mu\text{M}$  CAS treated wells at a volume of 400  $\mu\text{L}$ . After 20 h of incubation at 37°C, 5%  $\text{CO}_2$ , the chamber slide was rinsed gently with sterilized, deionized water to remove nonadherent cellular debris. Each well was then stained with 400  $\mu\text{L}$  FilmTracer™ SYPRO® Ruby Biofilm matrix stain according to the manufacturer's protocol. The chamber slide was then rinsed gently, and the chamber components were removed to allow visualization of the microscopic slide. 30  $\mu\text{L}$  of sterilized water was added to each well and then a coverslip was placed. The slide was then viewed under a Nikon Eclipse E600 microscope at 10x magnification utilizing a TRITC emission filter.

#### 4.15 Dose Dependence Reduction in Adherent Bacteria (IC<sub>50</sub> determination)

The same protocol for the culturing *S. mutans* UA159, dilutions and inoculation of a 96-well microtiter PS plate was followed as described above. A 5 mM stock solution of CAN was freshly prepared within 30 min of addition to the PS plate. The final volume of each well (test and controls) was 200  $\mu$ L. Both test wells and controls were run with six replicates. The loaded microtiter plate was placed in an incubator at 37 °C, 5% CO<sub>2</sub> for 20 h in the absence of light. The same workup described above for removing non-adherent cells/debris, staining with 0.1% CV, quantification of retained CV stain on the Victor3v plate (ABS570) was followed. The adherent bacteria reduction was determined by Equation III and plotted in Figure S1 as the mean  $\pm$  SD. The positive control was taken as the zero value for adherent bacteria reduction. Note negative control absorbances at 570 nm were subtracted from each positive control and test well value.

$$\text{Adherent Bacteria Reduction} = \left[ \frac{\left( \text{ABS}^{570}_{+\text{control}} - \text{ABS}^{570}_{\text{test well}} \right)}{\left( \text{ABS}^{570}_{+\text{control}} \right)} \right] \quad \text{Equation III}$$

#### 4.16 Bacterial Cell Viability Assay

A similar protocol for overnight culturing of *S. mutans* UA159 was also employed for *S. sobrinus* 6175. Each culture was separately grown to mid log phase and diluted 40-fold similarly to above. *S. mutans* and *S. sobrinus* were then exposed to 1 mM CAN, CAS or AgNO<sub>3</sub> from pre-dissolved 5 mM (metal ion) solutions and diluted accordingly into a 24 well PS plate. The plate was allowed to stand for 20 h at 37°C, 5% CO<sub>2</sub>. Well turbidity was judged visually and designated with a positive sign (++)

#### 4.17 Sucrose Metabolism Assay

A similar protocol for overnight culturing of *S. mutans* UA159 in BHI, and growing to mid log phase was followed as described earlier. A 4 mL culture was centrifuged down to a pellet at 4000 G (10 min). To the pellet was added 4 mL of PBS solution, vortexed for 30 s, and re-centrifuged for 10 min (4000G). The wash cycle was repeated 3x to rid the sample additional carbohydrates from BHI. Following the washing steps, the cell pellet was re-suspended in PBS to a final OD600 of 0.4. To a 45 mL of sterilized Phenol Red media was added the above PBS stock culture of *S mutans* (40 fold dilution). Each autoclaved borosilicate glass tube (13  $\times$  100 mm) was loaded with 2.85 mL of Phenol Red media (with or without 1% sucrose), 0.150 mL CAN, 0.150 mL CAS or 0.150 mL of DI water for the positive control to total a 5.0 mL solutions in each tube. The media was allowed to grow for 20 h at 37°C and 5% CO<sub>2</sub>. Media acidity measurements were taken at 5 and 20 h. At each measurement, 1 mL of media broth was removed, diluted with 1 mL of DI water and the pH was recorded with a Mettler Toledo FE20 benchtop pH meter. The average pH of the triplicate measurement are reported in Table S1 (*See Supplemental Data*).

#### 4.18 Biofilm Dispersal Assay

The same protocol for the culturing *S. mutans* UA159, dilution(s) and inoculation of a 96-well microtiter PS plate was followed as described above. The positive control and test wells

were prepared with a final volume of 200  $\mu$ L (BHI + cells) and the negative control was prepared with only 200  $\mu$ L BHI. The loaded microtiter plate was placed in an incubator at 37  $^{\circ}$ C, 5% CO<sub>2</sub> for 6 h in the absence of light. After 6 h, the planktonic cells were removed, the adherent biofilm rinsed (0.9% NaCl) and replaced with fresh 200 $\mu$ L BHI (controls) or BHI/500  $\mu$ M CAS (test wells). The same workup described above was used for removing non-adherent cells/debris, staining with 0.1% CV, quantification of retained CV on the Victor3v plate reader (ABS<sup>570</sup>) and calculation of adherent bacteria reduction (Equation III). Note negative control absorbances at 570 nm were subtracted from each positive control and test well value.

#### 4.19 Bacterial Cell Growth Curve

A similar protocol for the culturing of *S. mutans* UA159, dilutions and inoculation of a 96-well microtiter PS plate was followed as described above. Test agents included 500  $\mu$ M CAN and CAS and all test wells, positive and negative controls were run in triplicate. The OD<sub>600</sub> of each well was recorded every 30 min for 10 h on a Victor3v plate reader. The average OD<sub>600</sub> for each of the three triplicate runs (with standard deviation) was reported.

#### 4.20 Human Cell Proliferation Assays

3000 human telomerase immortalized gingival keratinocytes (TIGK, ATCC, Manassas, VA)/well were seeded in a 96-well plate in a culture medium (DermaLife K Medium Complete Kit, Lifeline Cell Technology) without the use of antibiotics. Two hours later, 10 mM stock solutions of CAN, CAS and AgNO<sub>3</sub> filtered through a 0.450  $\mu$ M filter were used to deliver concentrations ranging from 125–1000  $\mu$ M in the wells containing the cells were incubated for further 24 hours. Cells were cultured in an incubator at 37 $^{\circ}$ C in 5% CO<sub>2</sub> environment. Cells without the addition of any metal ions was used as the baseline control. Each treatment condition had three replicates. A cell proliferation assay was performed using CellTiter 96® Aqueous Non-Radioactive Cell Proliferation Assay kit (Promega, Madison, WI) per manufacturer's instructions. OD<sub>490</sub> was read using a spectrophotometer (SPECTRAMax Plus, Molecular Devices, San Jose, CA). A similar human cell proliferation assay utilizing the same metal containing solutions was carried out with primary human gingival fibroblasts (HGF, ATCC, Manassas, VA) cultured in a DMEM (ThermoFisher, Scientific, Catalog No. 11965) with 10% FBS.

### 5. Data Analysis

DLS, planktonic growth and dose dependent adherent bacteria reduction curves (IC<sub>50</sub>) were plotted on SigmaPlot (Systat Software Inc, San Jose, CA). All data utilizing bacteria were expressed as the mean  $\pm$  SD. The curve generated from the dose dependent adherent bacteria reduction assay was fit to the Hill equation (3-parameter) to arrive at the reported IC<sub>50</sub> value. Adherent bacteria and human cell proliferation data are expressed as means  $\pm$  SD and plotted on GraphPad (GraphPad Software Inc., San Diego, CA). The student t test (two way) analysis of all test substances were performed using GraphPad Prism software where p values < 0.05 were considered statistically significant.

## Supplementary Material

Refer to Web version on PubMed Central for supplementary material.

## Acknowledgements

We would like to thank the Electron Microscopy Service and the Nanotechnology Core Facility (Research Resources Center, UIC) for use of instrumentation required to complete this study. We also would like to thank Dr. Michael Johnson (UIC), Dr. Michael Federle (UIC) and Dr. Jeffrey Banas (University of Iowa) for comments regarding the preparation of this manuscript. We would like to thank Dr. Joanne Burdette (UIC) for allowing use of the Nikon Light Microscope in her laboratory and Dr. Luisa A. DiPietro (UIC) for allowing use of her laboratory for human cell toxicity studies. Also, we would like to thank Dr. Fengyuan Shi (UIC) for her assistance in collecting and interpreting HR-TEM images presented in this manuscript and Dr. Jordi Cabana for helpful discussion regarding the physical characterization of CeO<sub>2</sub>-NP. Finally, we would also like to thank Dr. Michael Federle for providing frozen glycerol stocks of *S. mutans* UA159 and *S. sobrinus* 6175. This work was supported by NIH/NIDCR Grants T32 DE018381 and 1K08DE028009-01A1 as well as the UIC Chancellor's Research Initiative Fund. The acquisition of the UIC JEOL JEM-ARM200CF was supported by the NSF MRI-R<sub>2</sub> grant (No. DMR-0959470), and the acquisition of the Gatan Continuum spectrometer was supported by a grant from the National Science Foundation MRI Program (No. DMR-1626065).

## Table of Abbreviations

6.

<b>BHI</b>	brain heart infusion
<b>TIFK</b>	human telomerase immortalized gingival keratinocytes
<b>CAN</b>	ceric ammonium nitrate
<b>HGF</b>	primary human gingival fibroblasts
<b>CAS</b>	ceric ammonium sulfate
<b>PS</b>	polystyrene
<b>CeO<sub>2</sub>-NP</b>	cerium oxide nanoparticles

## References

- [1]. Dewhirst FE, Chen T, Izard J, Paster BJ, Tanner AC, Yu WH, Lakshmanan A, Wade WG, J Bacteriol, vol. 192, 2010, pp. 5002–5017. [PubMed: 20656903]
- [2]. Klein MI, Hwang G, Santos PH, Campanella OH, Koo H, Front Cell Infect Microbiol, vol. 5, 2015, pp. 10. [PubMed: 25763359]
- [3]. Lemos JA, Palmer SR, Zeng L, Wen ZT, Kajfasz JK, Freires IA, Abranches J, Brady LJ, Microbiol Spectr, vol. 7, 2019.
- [4]. Davis IJ, Richards H, Mullany P, Oral Microbiol Immunol, vol. 20, 2005, pp. 191–194. [PubMed: 15836522]
- [5]. Mijndonckx K, Leys N, Mahillon J, Silver S, Van Houdt R, Biometals, vol. 26, 2013, pp. 609–621. [PubMed: 23771576]
- [6]. Allaker RP, Memarzadeh K, Int J Antimicrob Agents, vol. 43, 2014, pp. 95–104. [PubMed: 24388116]
- [7]. Hannig M, Hannig C, Nat Nanotechnol, vol. 5, 2010, pp. 565–569. [PubMed: 20581832]
- [8]. Thakur N, Manna P, Das J, J Nanobiotechnology, vol. 17, 2019, pp. 84. [PubMed: 31291944]
- [9]. Farias IAP, Dos Santos CCL, Sampaio FC, Biomed Res Int, vol. 2018, 2018, pp. 1923606. [PubMed: 29607315]

- [10]. Xu Y, Wang C, Hou J, Wang P, Miao L, You G, *Bioresour Technol*, vol. 265, 2018, pp. 102–109. [PubMed: 29885495]
- [11]. Xu Y, Wang C, Hou J, Wang P, Miao L, You G, Lv B, Yang Y, Zhang F, *Bioresour Technol*, vol. 245, 2017, pp. 573–580. [PubMed: 28910644]
- [12]. Lawrence JR, Paule A, Swerhone GDW, Roy J, Grigoryan AA, Dynes JJ, Chekabab SM, Korber DR, *Environ Pollut*, 2019, pp. 113515. [PubMed: 31706760]
- [13]. Garcia A, Delgado L, Tora JA, Casals E, Gonzalez E, Puntos V, Font X, Carrera J, Sanchez A, *J Hazard Mater*, vol. 199–200, 2012, pp. 64–72.
- [14]. Masadeh MM, Karasneh GA, Al-Akhras MA, Albiss BA, Aljarah KM, Al-Azzam SI, Alzoubi KH, *Cytotechnology*, vol. 67, 2015, pp. 427–435. [PubMed: 24643389]
- [15]. Xu Y, Wang C, Hou J, Wang P, You G, Miao L, *Environ Sci Pollut Res Int*, vol. 25, 2018, pp. 34765–34776. [PubMed: 30324376]
- [16]. Xu Y, Wang C, Hou J, Wang P, You G, Miao L, *Environ Sci Pollut Res Int*, vol. 26, 2019, pp. 9293–9304. [PubMed: 30725258]
- [17]. Nabavi M, Spalla O, Cabane B, *J Colloid Interf Sci*, vol. 160, 1993, pp. 459–471.
- [18]. Xu JX, Li GS, Li LP, *Mater Res Bull*, vol. 43, 2008, pp. 990–995.
- [19]. Pettinger NW, Williams RE, Chen J, Kohler B, *Phys Chem Chem Phys*, vol. 19, 2017, pp. 3523–3531. [PubMed: 28094375]
- [20]. Ikeda-Ohno A, Hennig C, Weiss S, Yaita T, Bernhard G, *Chemistry*, vol. 19, 2013, pp. 7348–7360. [PubMed: 23630017]
- [21]. Garcia SS, Blackledge MS, Michalek S, Su L, Ptacek T, Eipers P, Morrow C, Lefkowitz EJ, Melander C, Wu H, *J Dent Res*, vol. 96, 2017, pp. 807–814. [PubMed: 28571487]
- [22]. Walkey C, Das S, Seal S, Erlichman J, Heckman K, Ghibelli L, Traversa E, McGinnis JF, Self WT, *Environ Sci Nano*, vol. 2, 2015, pp. 33–53. [PubMed: 26207185]
- [23]. Matsumoto M, Minami T, Sasaki H, Sobue S, Hamada S, Ooshima T, *Caries Res*, vol. 33, 1999, pp. 441–445. [PubMed: 10529529]
- [24]. Xu FF, Bando Y, *J Appl Phys*, vol. 89, 2001, pp. 5469–5472.
- [25]. Wu LJ, Wiesmann HJ, Moodenbaugh AR, Klie RF, Zhu YM, Welch DO, Suenaga M, *Phys Rev B*, vol. 69, 2004.
- [26]. Shannahan J, *Nanotechnol Rev*, vol. 6, 2017, pp. 345–353. [PubMed: 29607287]
- [27]. Docter D, Westmeier D, Markiewicz M, Stolte S, Knauer SK, Stauber RH, *Chem Soc Rev*, vol. 44, 2015, pp. 6094–6121. [PubMed: 26065524]
- [28]. Jokisaari JR, Wang C, Qiao Q, Hu X, Reed DA, Bleher R, Luan X, Klie RF, Diekwisch TGH, *ACS Nano*, vol. 13, 2019, pp. 3151–3161. [PubMed: 30763075]
- [29]. Wang C, Shokuhfar T, Klie RF, *Adv Mater*, vol. 28, 2016, pp. 7716–7722. [PubMed: 27375052]
- [30]. Wang C, Qiao Q, Shokuhfar T, Klie RF, *Adv Mater*, vol. 26, 2014, pp. 3410–3414. [PubMed: 24497051]
- [31]. Ribeiro AR, Mukherjee A, Hu X, Shafien S, Ghodsi R, He K, Gemini-Piperni S, Wang C, Klie RF, Shokuhfar T, Shahbazian-Yassar R, Borojevic R, Rocha LA, Granjeiro JM, *Nanoscale*, vol. 9, 2017, pp. 10684–10693. [PubMed: 28654127]

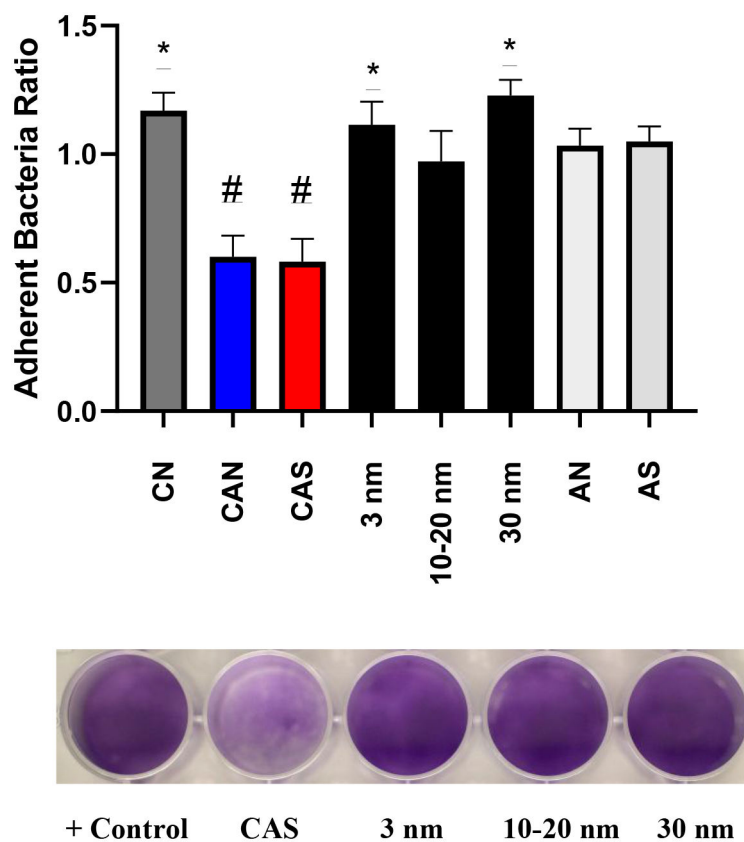


**Figure 1.** The ratio of adherent bacteria (compared to positive control) from the treatment of *S. mutans* UA159 with Ce-containing agents (125  $\mu$ M Ce) [CN =  $\text{Ce}(\text{NO}_3)_3 \cdot 6\text{H}_2\text{O}$ ] and ammonium salts (AN, AS) (1 mM BHI, 1% sucrose, 37°C, 5%  $\text{CO}_2$  for 20 h. \* $p < 0.05$ , # $p < 0.0001$ , student t test.

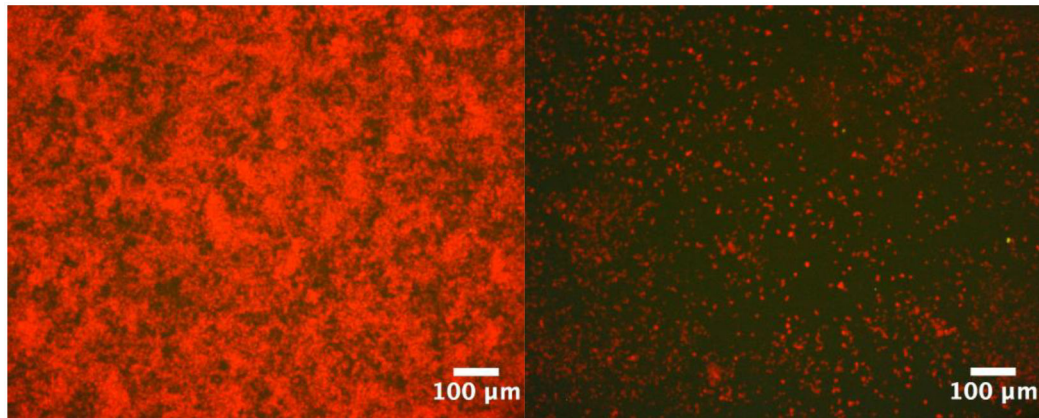


**Figure 2.** Microscopic images (10 x) of adherent *S. mutans* UA159 grown for 20 h at 37 °C, 5% CO<sub>2</sub> in BHI. The untreated wells (**left**) displayed significantly more biofilm growth than 250 μM CAS treated wells (**right**).

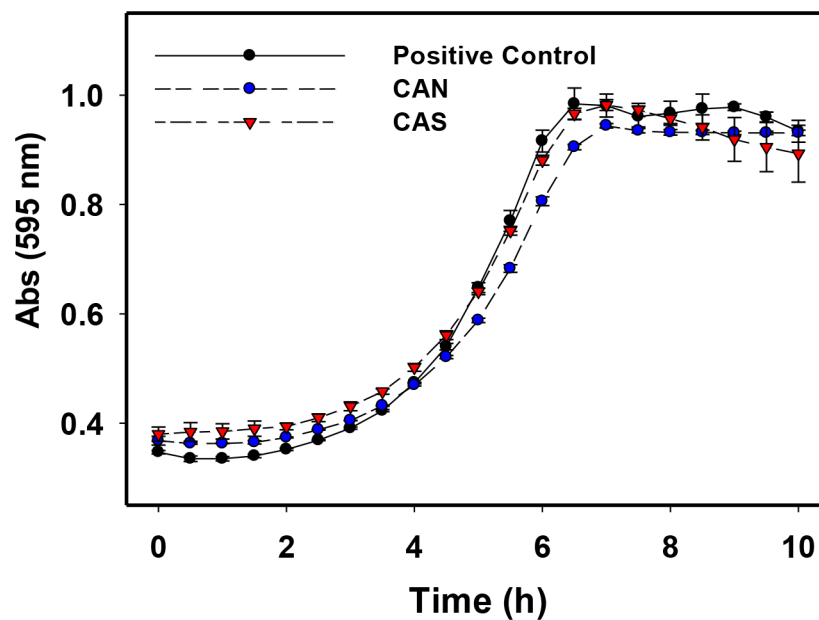


**Figure 3.** Planktonic growth curves of *S. mutans* UA159 with 500  $\mu$ M CAN and CAS treated cells in BHI at 37°C and 5% CO<sub>2</sub> for 10 h. Measurements were run in triplicate. Error bars represent standard deviation of the triplicate measurements.



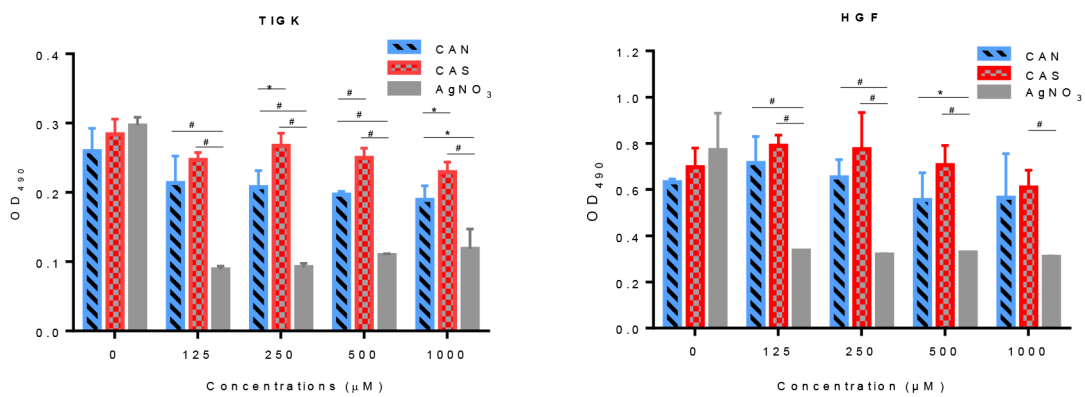


**Figure 4.** MTS cell proliferation assays utilizing **(left)** TIGK and **(right)** HGF in the presence of hydrolyzed CAN (red), CAS (blue) and AgNO<sub>3</sub> (gray) for 24 h at 37°C, 5% CO<sub>2</sub>. \*p<0.05, #p<0.01, t test.

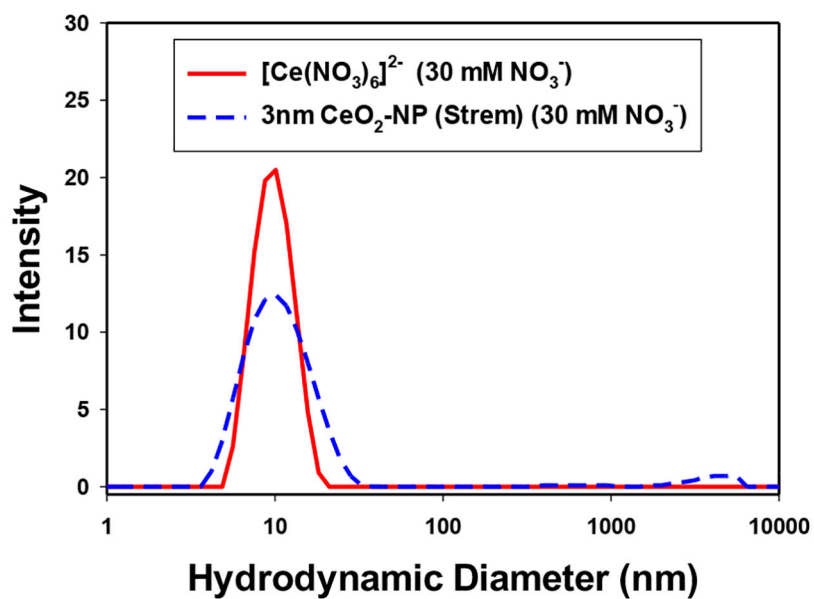


**Figure 5.** Distribution of hydrolyzed  $[\text{Ce}(\text{NO}_3)_6]^{2-}$  (pH 1.8) and  $\text{CeO}_2$ -NP (3 nm, Strem) (pH 4.5) in 30 mM  $\text{NO}_3^-$ .

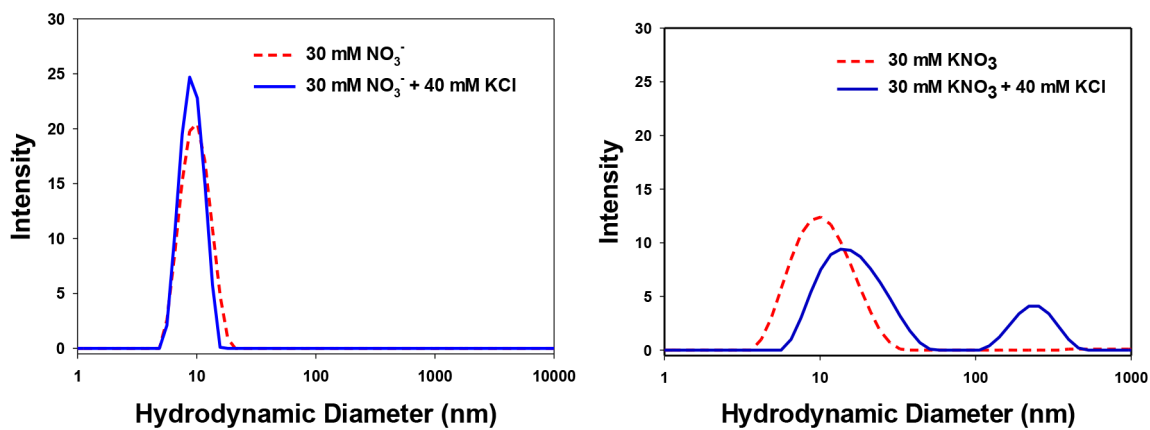


**Figure 6.** Distribution of (left) 5 mM  $[\text{Ce}(\text{NO}_3)_6]^{2-}$  (pH 1.8) and (right) 5 mM  $\text{CeO}_2$ -NP (3 nm, Strem) (pH 4.5) in 30 mM  $\text{NO}_3^-$  and with 40 mM KCl.

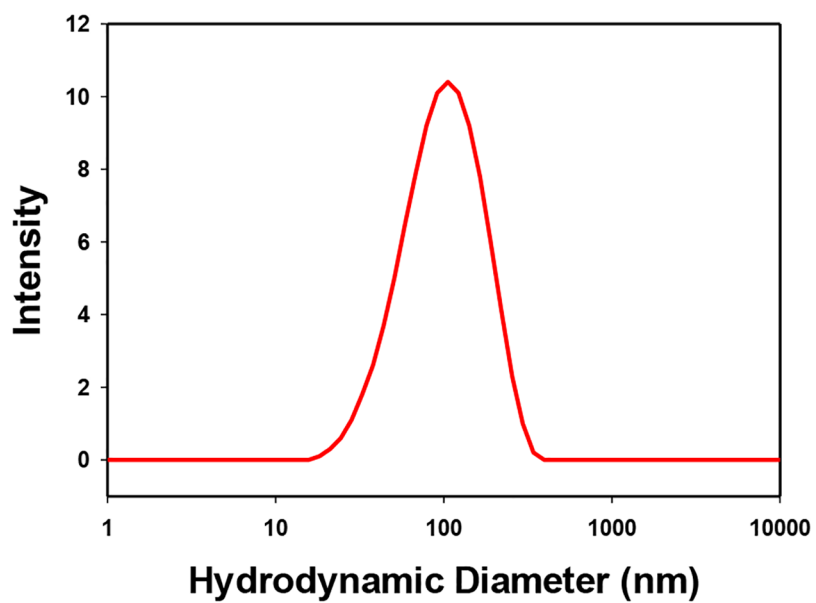


**Figure 7.**  
Distribution of hydrolyzed  $[\text{Ce}(\text{NO}_3)_6]^{2-}$  ( $500 \mu\text{M}$  Ce) in  $50 \text{ mM}$   $\text{KH}_2\text{PO}_4$  (pH 7.4)

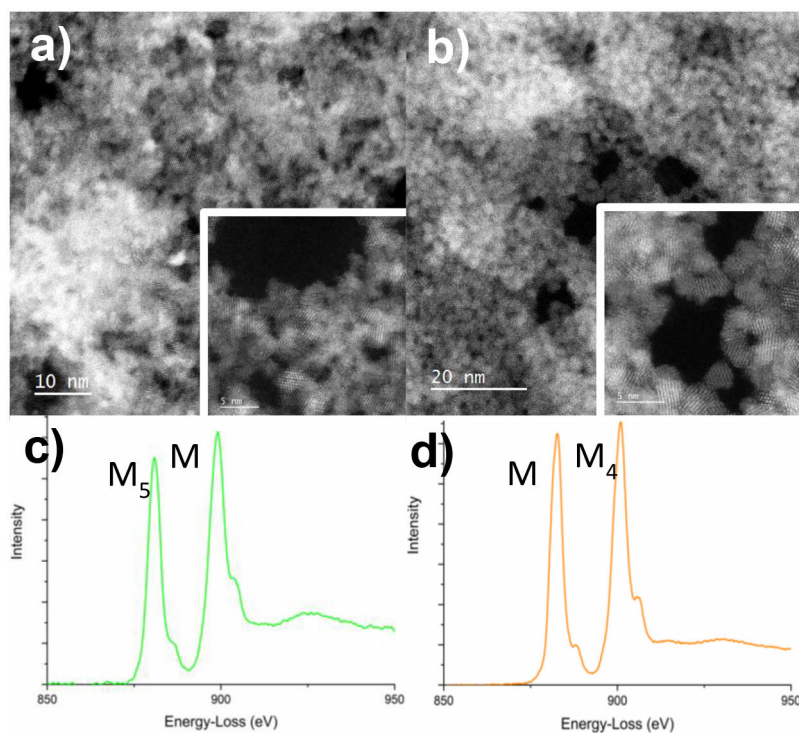


**Figure 8.** Low-magnification high-angle annular dark field (HAADF) of (a) hydrolyzed  $[\text{Ce}(\text{NO}_3)_6]^{2-}$  and (b)  $\text{CeO}_2$ -NP (3nm, Strem) in graphene liquid cells. Inserts show high-resolution images of the nano-particles revealing lattice fringes. Electron energy-loss spectroscopy (EELS) of the Ce M-edges for (c) hydrolyzed  $[\text{Ce}(\text{NO}_3)_6]^{2-}$  and (d)  $\text{CeO}_2$ -NP (3nm, Strem) in graphene liquid cells, showing the  $M_4/M_5$  ratio expected for a Ce(IV) valence state.

**Table 1.**

Planktonic Cell Viability Assay with 1 mM Metal Ion

<b>BHI, 37 °C, 5% CO<sub>2</sub>, 20 h</b>	<b>OD600</b>	<b>CAN</b>	<b>CAS</b>	<b>AgNO<sub>3</sub></b>
<i>S. mutans</i>	0.010	++	++	--
<i>S. sobrinus</i>	0.010	++	++	--

Author Manuscript

Author Manuscript

Author Manuscript

Author Manuscript